

with wave vectors near the Brillouin zone boundary; such zone-boundary phonons generally have the large electric fields postulated in the present model. Assertion (ii) assumes that the internal fields are the same order of magnitude in I-VII, II-VI, and III-V compounds; in fact, the more ionic solids generally have larger internal fields. When the dependence of internal fields on dielectric function is taken into account in the Frohlich model [Eq. (c16)], we find that the Urbach exponent (which apart from numerical constants is  $E/\bar{f}$ ) becomes

$$\frac{E}{\bar{f}} = \frac{\hbar\omega - E_{g0}}{k_B T^*} \frac{\sqrt{3}}{4(\epsilon_0/\epsilon_\infty - 1)}$$

Here we have used the relationship  $q_0 a \sim (V_{\text{rms}}/R)^{1/2}$ , as discussed in Eq. (13). Note that this is precisely the observed Urbach dependence, with the additional prediction of the variation of  $\sigma$  with  $\epsilon_0$  and  $\epsilon_\infty$ :  $\sigma \propto (\epsilon_0/\epsilon_\infty - 1)^{-1}$ . This slight variation of  $\sigma$  is the observed one (the more

ionic systems have smaller values of  $\sigma$ ). However, we caution the reader that this last prediction may depend on the *ad hoc* manner in which the wave-vector cutoff has been introduced; furthermore, the data on  $\sigma$  are not unambiguous on this question.

<sup>90</sup>J. D. Dow, Comments Solid State Phys. (to be published).

<sup>91</sup>H. Fritzsche, J. Noncrystalline Solids **6**, 49 (1971); J. Tauc, *ibid.* (to be published).

<sup>92</sup>J. D. Dow and J. J. Hopfield (unpublished); see also Ref. 42.

<sup>93</sup>M. DiDomenico and S. H. Wemple, Phys. Rev. **166**, 565 (1968).

<sup>94</sup>A. B. Fowler, W. E. Howard, and G. E. Brock, Phys. Rev. **128**, 1664 (1962).

<sup>95</sup>T. G. Castner and W. Känzig, J. Phys. Chem. Solids **3**, 178 (1957).

<sup>96</sup>A. Messiah, *Quantum Mechanics* (Wiley, New York, 1961), p. 449.

## Photoconductivity Due to Excitonic-Energy Transfer to Crystalline Defects\*

W. L. Emkey† and W. J. Van Sciver

Department of Physics, Lehigh University, Bethlehem, Pennsylvania 18015

(Received 23 July 1971)

The internal photoconductivity spectrum of single crystals of NaI was investigated over a wide range of temperatures. A photocurrent threshold was observed which is believed to be due to the onset of band-to-band transitions. Aside from this threshold, a photoconductivity band appeared on the low-energy side of the first fundamental absorption band. The existence of this response is attributed to the ionization of traps via an exciton interaction.

### I. INTRODUCTION

Early work on the intrinsic photoconductivity of single crystals of KI, KBr, and KCl by Kuwabara and Aoyagi<sup>1</sup> indicated that, aside from photocurrents due to band-to-band transitions, a photoconductivity response appeared on the low-energy tail of the first fundamental absorption band. They attributed this response either to an absorption related to the presence of an impurity or to impurity ionization via an exciton energy transfer. Their results favored the latter mechanism. At the same time, Nakai and Teegarden<sup>2</sup> reported results on the photoconductivity of RbI and KI single crystals. Once again, aside from band-to-band related photocurrents, an additional band was observed on the low-energy tail of the corresponding fundamental absorption spectrum. The authors postulated the photoproduction and destruction of color centers as being responsible for this band, and they indicated the *F* center as a possible candidate. In this paper, we present the results of our photoconductivity studies of NaI and RbI in the corresponding spectral region.

### II. EXPERIMENTAL PROCEDURE

Single crystals, obtained from the Harshaw Chemical Co., were cleaved in a dry box. These crystals, typically of 1.0-mm thickness, were then mounted onto the sample holder, a diagram of which can be seen in Fig. 1. The sample holder was attached to the end of a  $\frac{7}{8}$ -in. stainless-steel tube which was then inserted into the sample chamber of an Andonian exchange-gas cryostat. Because of the design of the cryostat, it was necessary for the signal to travel a distance of  $\sim 3$  ft before the photocurrent detection system could be connected. Because of the electrical noise involved due to the generation of microphonics, a  $\frac{1}{8}$ -in.-brass rod was used as the signal "wire." This rod, which was held in place by Teflon spacers within the stainless-steel tube, was found to effectively reduce the microphonics.

Photocurrents were detected by a Keithley model No. 640 electrometer with the input shunted by  $10^{12} \Omega$ . An electric potential of 800 V was supplied by a combination of dry-cell batteries. Data were acquired by first recording a background current.

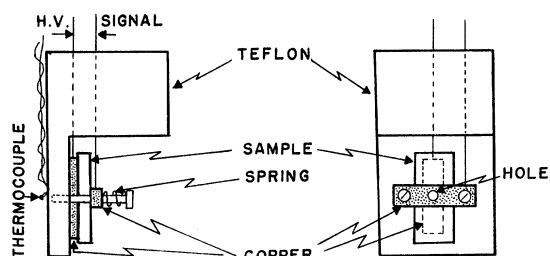


FIG. 1. Sample holder.

This current was just the current present when the exciting monochromator was set at a wavelength which was not transmitted by the quartz optics. The background current was subtracted from the measured photocurrent in order to arrive at the actual photocurrent. In all the measurements reported here, the samples were at atmospheric pressure in an atmosphere of either dry nitrogen or dry helium gas dependent upon whether liquid nitrogen or liquid helium was used as the cooling agent.

### III. RESULTS

Figure 2 shows a typical photoconductivity spectrum of NaI as observed at  $10^\circ\text{K}$ . For the sake of comparison, Fig. 2 contains two curves. The dashed curve is the liquid-helium temperature fundamental absorption spectrum<sup>3</sup> and is referred to the linear scale of optical density. The solid curve is the observed photoconductive response and is referred to the logarithm scale of photocurrent.

Several features of the photoconductivity spectrum can be noted. At low energies one can see

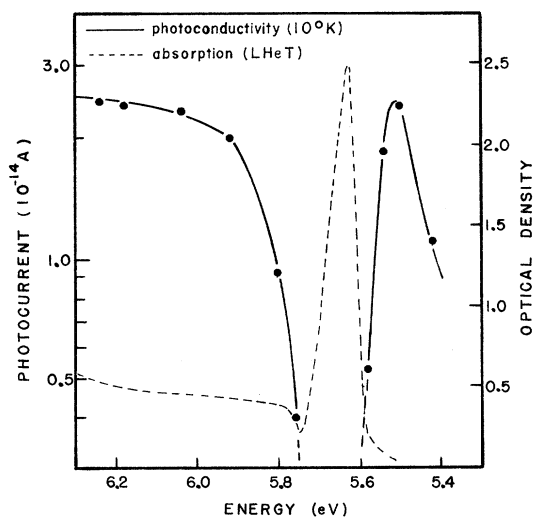


FIG. 2. Photoconductivity spectrum of NaI at  $10^\circ\text{K}$  and the fundamental absorption spectrum of NaI at liquid-helium temperature (Ref. 3).

the appearance of a photoconductivity band. This band occurs slightly on the low-energy side of the first fundamental absorption band. In addition, coinciding with the position of this first absorption band is a minimum in the photoconductive response. A photocurrent threshold is also evident at about 5.8 eV.

The photoconductivity spectrum of NaI as observed at  $80^\circ\text{K}$  is given in Fig. 3. The fundamental absorption spectrum at liquid-nitrogen temperature<sup>4</sup> is also shown here.

The low-energy photoconductivity band has increased in magnitude and shifted to lower energies as compared to the  $10^\circ\text{K}$  spectrum. Once again, a minimum in the response is found to coincide with the position of the first fundamental absorption band. In addition, a photocurrent threshold is seen at about 5.7 eV.

The photoconductive response in the low-energy tail of the first fundamental absorption band of NaI was investigated for a single crystal over a wide range of temperatures. The results of this investigation are given in Fig. 4. The curves indicate that as the temperature increases a monotonic shift of the band toward lower energies occurs. The intensity of the band increases as the temperature increases to about  $218^\circ\text{K}$ . Above this value, it is seen that the efficiency of the low-energy band decreases.

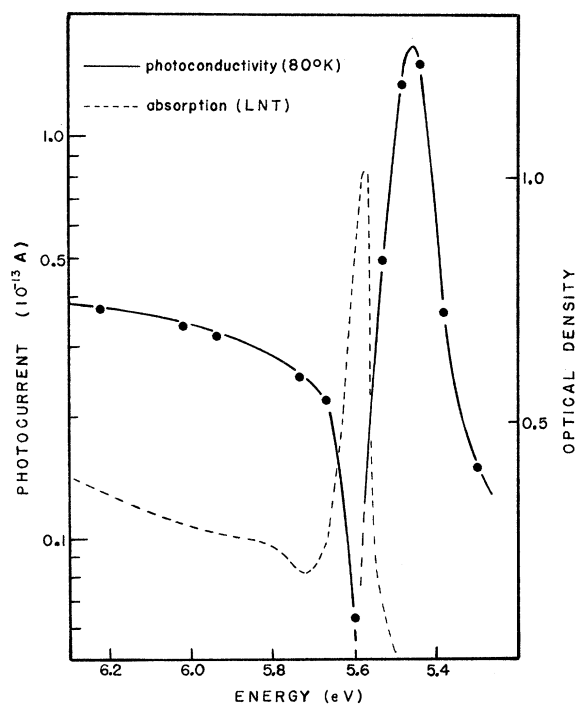


FIG. 3. Photoconductivity spectrum of NaI at  $80^\circ\text{K}$  and the fundamental absorption spectrum of NaI at liquid-nitrogen temperature (Ref. 4).

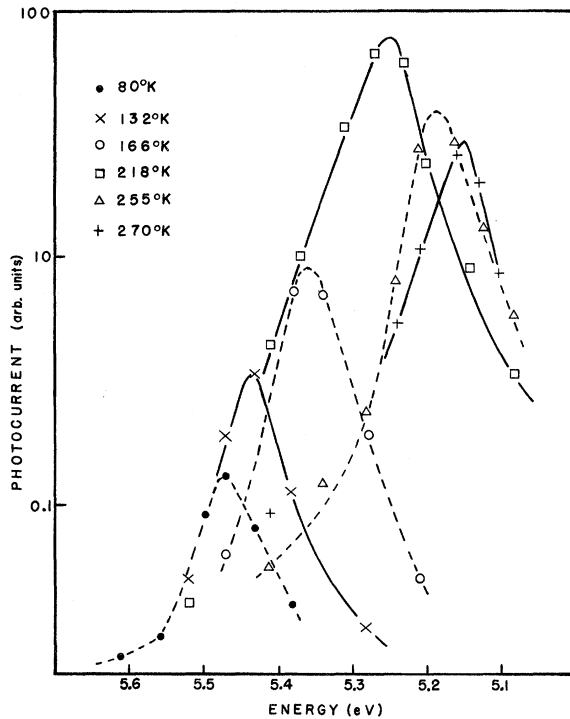


FIG. 4. Temperature-dependent behavior of the low-energy photoconductivity band in NaI.

The half-width of the band remains constant and has a value of 0.1 eV over the entire temperature range investigated. This effect is demonstrated by Fig. 5, in which the low-energy band as observed at various temperatures is plotted. The curves were normalized to give the same peak intensity, and their energy scales shifted to superimpose their peaks. The resulting collection of points demonstrates the lack of any significant deviation from a constant half-width of about 0.1 eV over the indicated temperature range.

The photoconductivity exhibited a linear response with respect to the magnitude of the applied electric field. This linear behavior occurred for irradiation at high energies ( $> 6.0$  eV) as well as for irradiation in the region of the low-energy photoconductivity band. In addition, the photocurrent as a function of exciting light intensity was determined to be linear.

#### IV. ANALYSIS OF RESULTS

Both Figs. 2 and 3 show photoconductivity thresholds (at  $\sim 5.8$  eV) which is in close agreement with the corresponding position of the optical absorption "step." It is this threshold which is attributed to the onset of electronic band-to-band transitions associated with excitation of electrons situated at the  $\Gamma$  point in the first Brillouin zone of the uppermost valence band.

The first fundamental absorption band is associated with the creation of excitons. Since the exciton is an electrically neutral entity, the absorption of light resulting in their formation is expected to yield a minimum in the photoconductive response. This is the condition which was observed in the photoconductivity spectra at energies corresponding to the first fundamental absorption band.

The existence of the low-energy photoconductivity band is attributed to the ionization of shallow traps via an exciton interaction. This model was first proposed by Kuwabara and Aoyagi.<sup>1</sup> We will base our analysis on the work of DeVore,<sup>5</sup> who performed calculations to determine the equilibrium concentration of electron-hole pairs in photoconductors.

The equilibrium concentration of pairs (excitons, in our case) is determined at some point within a photoconductor of thickness  $l$ . The calculations are based upon the following conditions: (a) constant irradiation of the sample with a photon intensity  $I$  (photons/sec), (b) each absorbed photon produces a pair, (c) a monomolecular recombination rate within the bulk, (d) a diffusion rate associated with the pairs, and (e) boundary conditions based on a recombination current at each of the surfaces. Since we are considering here the creation of excitons, we will refer to pairs as excitons and, for the sake of clarity, the term "recombination" will

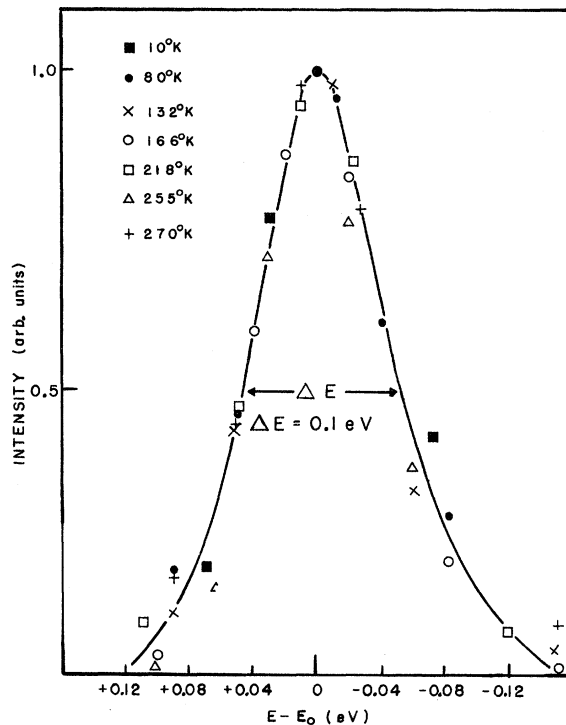


FIG. 5. Temperature dependence of the half-width of the low-energy photoconductivity band in NaI.

be referred to as annihilation. The extension of DeVore's analysis is well suited to our case in several respects. Photocurrents were measured by constant irradiation of the samples. In addition, the annihilation rate of excitons is known to obey a monomolecular law. The existence of an applied electric field is not considered in the analysis. Since the exciton is an electrically neutral entity, the omission of this consideration is particularly applicable to our experiments. Using these conditions, an equilibrium concentration of excitons,  $n(x)$ , is then determined. The parameters incorporated in  $n(x)$  are the diffusion constant  $D$ , the absorption coefficient  $\alpha$ , the bulk lifetime  $\tau$ , and a surface annihilation velocity  $S$ . Assuming that the photoconductivity is proportional to the total number of excitons present, this number is then determined by

$$N = \int_0^l n(x) dx,$$

which yields

$$N = \frac{\tau I}{1 - \xi^2} \left( (1 - e^{-\lambda \xi}) - \frac{\xi \xi (1 + e^{-\lambda \xi}) + \xi^2 (1 - e^{-\lambda \xi})}{1 + \xi \coth \frac{1}{2} \lambda} \right).$$

The parametric definitions made by DeVore are

$$l/(D\tau)^{1/2} \equiv \lambda \quad (\sim \text{thickness of photoconductor}),$$

$$\alpha(D\tau)^{1/2} \equiv \xi \quad (\sim \text{absorption coefficient}),$$

$$S(\tau/D)^{1/2} \equiv \xi \quad (\sim \text{ratio of surface-to-volume recombination rates, equivalent in our case to exciton annihilation rates}).$$

By redefining  $z \equiv \lambda \xi = \alpha l$  and by writing the photoconductivity in the form  $P = N/I\tau$ , we arrive at a final expression:

$$P = \frac{1 - e^{-z}}{1 + \xi \coth \frac{1}{2} \lambda} \left( 1 + \frac{\xi \lambda (\lambda \coth \frac{1}{2} \lambda - z \coth \frac{1}{2} z)}{\lambda^2 - z^2} \right).$$

DeVore proceeds to analyze several limiting cases. In particular, it was found that as the ratio of surface-to-volume annihilation rates  $\xi$  increased, a photoconductivity band would appear at some given value of the absorption coefficient. For the condition  $\xi \gg 1$ , the photoconductivity equation reduces to

$$P = \frac{1 - e^{-z}}{\xi} \left( 1 + \frac{\xi \lambda}{\lambda + z} \right).$$

The value of  $\alpha$  for which the photocurrent maximizes is obtained by setting  $\partial P/\partial z = 0$ . The peak position is then determined by the appropriate values of the involved parameters. In any case, for a single crystal this peak occurs at an absorption coefficient which would appear on the tail of the fundamental absorption spectrum.

The above analysis appears to be applicable to

our case if one considers the experimental evidence available which demonstrates exciton migration and interaction with impurities or defects. In addition, the peak position of the observed photoconductivity band is also consistent with the model. The analysis between the experimental observations and the above theory can be carried even further. Specifically, a prediction can be made as to the energy location of the photoconductivity band as a function of temperature using DeVore's analysis in conjunction with the behavior of the absorption coefficient in the low-energy tail of the first fundamental absorption band.

To the best of the authors' knowledge, no detailed analysis is available on the absorption coefficient in the low-energy tail of NaI. It has been found, however, that in several other alkali halides the structure in this region can be closely approximated by Urbach's rule.<sup>6-8</sup> According to Urbach's rule,

$$\alpha = \alpha_0 \exp[\sigma(E - E_0)/kT^*],$$

where

$$T^* = T_0 \coth(T_0/T),$$

$\alpha$  is the absorption coefficient at some energy  $E$ ,  $T$  is the temperature ( $^{\circ}$  K), and the other quantities are constants. Solving the above for  $E$ , we get

$$E = (kT^*/\sigma) \ln(\alpha/\alpha_0) + E_0,$$

or in terms of  $T$

$$E = (kT_0/\sigma) \ln(\alpha/\alpha_0) \coth(T_0/T) + E_0.$$

The prediction of DeVore's theory is that the photoconductivity band's peak position is determined by some given value of  $\alpha$ . Using this premise, then, the energy is calculated from the latter equation over a range of temperatures, keeping the value of  $\alpha$  constant. The results of this calculation are then compared to the experimentally obtained peak positions of the low-energy photoconductivity band. This comparison is indicated in Fig. 6. As can be seen, close agreement is obtained between the experimental points and the curve describing the calculated values. In the calculation, it was necessary to assign appropriate values to  $(T_0/\sigma) \ln(\alpha/\alpha_0)$  and  $E_0$ . The fit in Fig. 6 was obtained with  $E_0 = 5.6$  eV and with a value for  $(T_0/\sigma) \ln(\alpha/\alpha_0)$  which could be broken down into  $T_0 = 60^{\circ}$  K,  $\sigma = 0.65$ , and  $\alpha/\alpha_0 = 10^{-5}$ . These parametric values are consistent with the values used for the alkali halides whose structure in this region has been analyzed.<sup>8</sup>

It will be recalled that the half-width of the low-energy photoconductivity band remained essentially constant at 0.1 eV over the range of temperatures investigated. The following discussion demonstrates the consistence of this observation with the analysis put forth by DeVore. The predicted photoconductivity curves<sup>5</sup> indicate that the half-width is

determined by the difference in the absorption coefficient at half-height. If one assumes that there is a negligible temperature dependence of the parameters involved in the calculation, then the half-width should be determined by some constant  $\Delta\alpha$ .

The half-width of a band (in terms of  $\alpha$ ) is  $\alpha_2 - \alpha_1 \equiv \Delta\alpha$ . From Urbach's rule this corresponds to

$$\Delta\alpha = \alpha_0 \left[ \exp\left(\frac{\sigma(E_2 - E_0)}{kT^*}\right) - \exp\left(\frac{\sigma(E_1 - E_0)}{kT^*}\right) \right],$$

and at another effective temperature denoted by  $T^{*'}$  we have

$$\Delta\alpha' = \alpha_0 \left[ \exp\left(\frac{\sigma(E_2' - E_0)}{kT^{*'}}\right) - \exp\left(\frac{\sigma(E_1' - E_0)}{kT^{*'}}\right) \right].$$

By substituting for  $E_2 = E_1 + \Delta E$  and for  $E_2' = E_1' + \Delta E'$  and by equating  $\Delta\alpha = \Delta\alpha'$  we arrive at

$$\begin{aligned} \exp\left(\frac{\sigma(E_1 - E_0)}{kT^*}\right) (e^{\sigma\Delta E/kT^*} - 1) \\ = \exp\left(\frac{\sigma(E_1' - E_0)}{kT^{*'}}\right) (e^{\sigma\Delta E'/kT^{*'}} - 1), \end{aligned}$$

where  $\Delta E$  and  $\Delta E'$  are the energy half-widths at the two different temperatures. A valid approximation at these temperatures is

$$e^{\sigma\Delta E/kT^*} \gg 1.$$

Utilizing this approximation and further reducing the equation the result is, upon solving for  $E_0$ ,

$$E_0 = \frac{T^{*'}(E_1 + \Delta E) - T^*(E_1' + \Delta E')}{T^{*'} - T^*}.$$

The self-consistency of the model is checked by inserting into the latter equation the appropriate experimental values in order to determine the constant  $E_0$ . In the calculations  $\Delta E = \Delta E' = 0.1$  eV for all temperatures,  $E_0$  was calculated by using the parameters of the 10° K results with the parameters as obtained from the higher-temperature curves (Fig. 6). These calculations were also performed using the 80° K results with the appropriate parameters from the higher-temperature curves. Table I gives the computed values of  $E_0$  determined by

TABLE I. Calculated values of  $E_0$  using the experimental parameters of the indicated temperatures.

$T$ (°K)	10	80
10	...	5.60
80	5.60	...
132	5.58	5.56
166	5.62	5.65
216	5.60	5.60
255	5.63	5.63
270	5.65	5.68
$E_0$ (av)	5.61	5.62

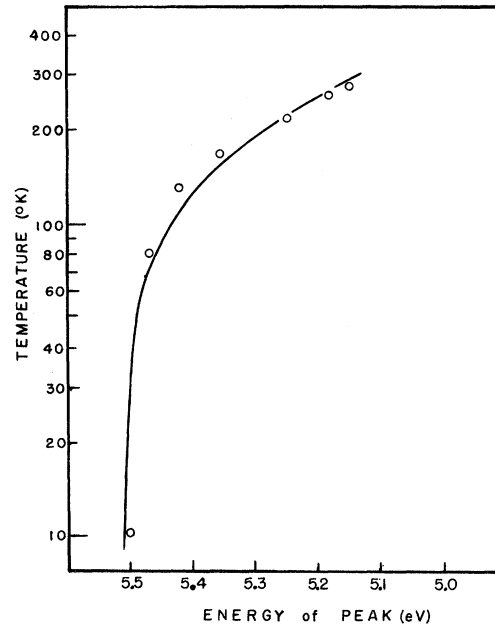


FIG. 6. Theoretical-experimental comparison of the peak position of the low-energy band as a function of temperature.

using the experimental parameters of the temperatures indicated.

It will be recalled that the value of  $E_0$  used in the theoretical fit of Fig. 6 was 5.6 eV. As the calculations are extended to include the parameters associated with the higher-temperature observations, the agreement with  $E_0$  becomes poorer. However, all sets of calculations yield an average value of

$$E_0 = 5.6 \text{ eV} \pm 3\%.$$

Additional support for the applicability of DeVore's calculations is realized if one considers the case of thin photoconductors. In the limit as  $\lambda \rightarrow 0$ , we have

$$P \sim (\lambda/2\xi)(1 - e^{-\lambda}).$$

This equation predicts that no peak will be observed in the photoconductive response. In the photoconductivity study of thin films by Huggett and Teegarden<sup>9</sup> no low-energy band was reported for samples which did possess this band in a single-crystal state.<sup>1,2</sup> However, they do report a photoconductive band on the high-energy side of the first fundamental absorption band. That this is, in fact, a separate response is verified later in this paper.

Some earlier explanations accorded the low-energy band were based upon a photoproduction and destruction of defect centers, the  $F$  center being a possible candidate.<sup>2</sup> This possibility was based partially on an observed nonlinear dependence of the photocurrent in this region with respect to the

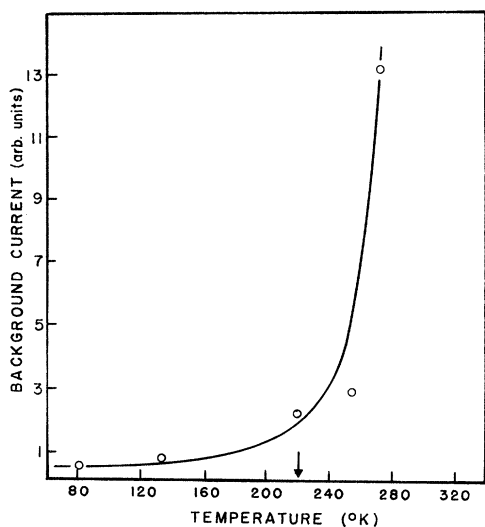
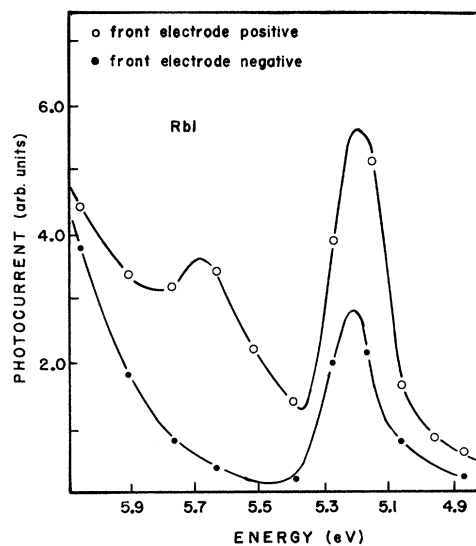


FIG. 7. Background current as a function of temperature.

incident light intensity. In the work reported here, a linear response was observed. In addition, it is felt that this explanation does not pertain to NaI because of the stability exhibited by the material under prolonged ultraviolet irradiation and because of its virtual immunity to the creation of  $F$  centers by high-energy irradiation.

We suggest that the decrease in the photocurrent intensity at temperatures above  $218^{\circ}\text{K}$  is due to a thermal ionization of shallow traps which, at lower temperatures, contribute to the photoconductivity. If this thermal ionization does occur, and if it is a large enough effect, one should be able to see it as an increase in the background current, the back-

FIG. 9. Effect of polarity reversal on the photoconductivity response of RbI at  $250^{\circ}\text{K}$ .

ground current being just the current present in the absence of any exciting light. Such an effect was observed and can be seen in Fig. 7. The arrow in Fig. 7 indicates the temperature above which the photoconductivity decreases. The proposed explanation appears to be consistent with the abrupt increase in the background conductivity in the vicinity of this temperature. It is also noted here that the reduction of the photoconductive response at higher temperatures is not believed to be attributable to a "field blocking" caused by an increase in the ionic mobility. One would expect that if the effective electric field were reduced by this ionic space charge, then

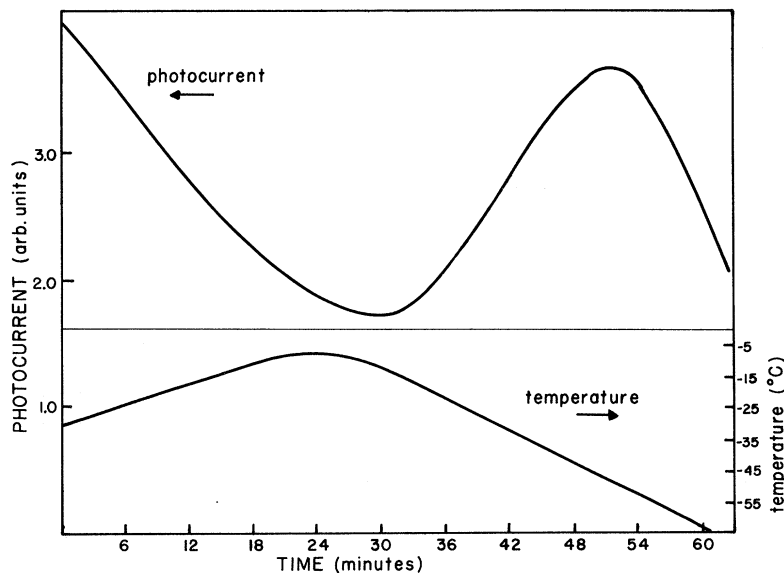


FIG. 8. Continuous temperature dependence of the low-energy band photocurrent with the electric field applied.

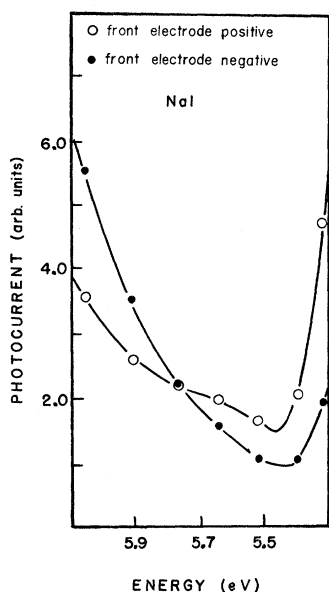


FIG. 10. Effect of polarity reversal on the photoconductivity response of NaI at 250 °K.

the reduced field would be frozen in as the temperature is lowered while the field is still applied. To see if this condition existed, the photocurrent was monitored continuously as a function of time as the temperature was raised and then lowered through the temperature region of interest. During this experiment, the electric field was applied at all times. The results of this experiment are given in Fig. 8. As Fig. 8 indicates, the temperature-dependent behavior of the photoconductivity appears to be independent of the direction of the changing temperature. Specifically, there is no indication of freezing in some reduced field as the temperature is lowered.

It was mentioned above that the spectral response of thin-film photoconductivity measurements indicated a band appearing at energies below the band-to-band threshold. Sydor<sup>10,11</sup> had demonstrated, for RbI, that this response is due to a surface conductivity resulting from exciton migration and subsequent interaction with surface states. One of the observations upon which this conclusion was based was that the band appeared only when the illuminated surface of the crystal was at the positive potential. This was true for single crystals of appropriate thickness. That this response is different from the photoconductivity band reported here is verified by

our experiments conducted on RbI. The photoconductivity spectrum of a single crystal of RbI at 250 °K is given in Fig. 9 for two different polarities. These results show the simultaneous appearance of both photoconductivity bands when the illuminated side of the crystal is at the positive potential.

The effects of polarity reversal on the photoconductivity spectrum of NaI were also investigated. The results obtained could not conclusively verify the existence of a second photoconductivity band. A typical photoconductivity spectrum under both polarities is given in the 250 °K response of Fig. 10.

## V. SUMMARY

A photoconductivity band was observed on the low-energy tail of the first fundamental absorption band in both NaI and RbI. This band had the following characteristics: (i) a monotonic shift to lower energies with increasing temperature, (ii) an increase in intensity of over two orders of magnitude as the temperature was raised from 10 to 218 °K, (iii) a decrease in intensity as the temperature was raised above 218 °K, and (iv) a constant half-width of 0.1 eV over the entire temperature range investigated.

The existence of this band is believed to be due to the ionization of shallow traps within the bulk of the crystal as a result of an exciton interaction. A combination of DeVore's theory<sup>5</sup> and Urbach's rule<sup>6,7</sup> is used to describe the position of the band as well as its temperature dependence. It was found that the constant half-width was consistent with the analysis. The reduction in the efficiency of the band at high temperatures is thought to be due to a reduction in the number of shallow-trapped electrons as a consequence of thermal ionization.

That there exist two photoconductivity bands in the region of the first fundamental absorption band was demonstrated in the case of RbI. It was found that aside from the low-energy response, a second response appeared on the high-energy side of the first fundamental absorption band. This second band occurred only when the illuminated surface was at the high potential and is believed to be the same response as has been previously analyzed by Sydor.<sup>10,11</sup>

## ACKNOWLEDGMENTS

The authors wish to thank Dr. W. Beall Fowler and Dr. Frank J. Feigl for their helpful discussions and suggestions during the course of this research.

\*Work supported by the U. S. Atomic Energy Commission Contract No. AT(30-1)-3408.

†Present address: Pennsylvania State University, Allentown Campus, Fogelsville, Pa.

<sup>1</sup>G. Kuwabara and K. Aoyagi, *J. Phys. Chem. Solids*

*22*, 333 (1961).

<sup>2</sup>Y. Nakai and K. Teegarden, *J. Phys. Chem. Solids*

*22*, 327 (1961).

<sup>3</sup>K. J. Teegarden and G. Baldini, *Phys. Rev.* *155*, 896 (1967).

<sup>4</sup>J. E. Eby, K. J. Teegarden, and D. B. Dutton, *Phys. Rev.* **116**, 1099 (1959).

<sup>5</sup>H. B. DeVore, *Phys. Rev.* **102**, 86 (1956).

<sup>6</sup>F. Urbach, *Phys. Rev.* **92**, 1324 (1953).

<sup>7</sup>D. L. Dexter, *Nuovo Cimento* **7**, 245 (1958).

<sup>8</sup>W. Martienssen, *Phys. Chem. Solids* **2**, 257 (1957).

<sup>9</sup>G. R. Huggett and K. Teegarden, *Phys. Rev.* **141**, 797 (1966).

<sup>10</sup>M. Sydor, *Phys. Rev.* **163**, 873 (1967).

<sup>11</sup>M. Sydor, *Phys. Rev.* **183**, 846 (1969).

PHYSICAL REVIEW B

VOLUME 5, NUMBER 2

15 JANUARY 1972

## Noncollinear Attenuation of Transverse Acoustic Waves in $\text{Al}_2\text{O}_3$ <sup>†</sup>

R. C. Purdom\*

*Department of Physics, Purdue University, Lafayette, Indiana 47907*  
*and Department of Physics and Mathematics, Kentucky Wesleyan College, Owensboro, Kentucky 42301*

and

E. W. Prohofsky

*Department of Physics, Purdue University, Lafayette, Indiana 47907*

(Received 28 July 1971)

For transverse waves propagated along an even-fold axis, the phonon-phonon coupling parameters are zero for collinear interactions. This necessitates a consideration of the angular dependence of the coupling parameter. The angle at which these parameters peak affects the minimum energy deficit possible on interactions. A calculation including both the angular dependence of the coupling parameters and the uncertainty of phonon energy due to thermal-phonon lifetimes is done for the case of  $\text{Al}_2\text{O}_3$  along the  $a$  axis. The calculated attenuation fits the experimentally observed attenuation.

### I. INTRODUCTION

The agreement of theoretical calculations of ultrasonic attenuation in insulators at low temperatures with experimental observation has greatly improved since the uncertainty in energy of the thermal phonons has been included.<sup>1,2</sup> This uncertainty in energy arises because of the extremely short lifetime of thermal phonons due to their interactions with other thermal phonons and/or defects. The uncertainty in energy allows processes to occur which are not included in the Golden Rule calculation of Landau and Rumer.<sup>3</sup>

Although these non-energy-conserving processes are reduced in probability over strictly conserving processes, in many materials no conserving processes are possible, and in addition there are so many such nonconserving processes possible that their total effect on the attenuation can be the greater. In such cases one can get attenuation considerably different than that predicted by Landau and Rumer.

In this paper, we consider the measurements by de Klerk<sup>4</sup> of the attenuation along an even-fold axis in  $\text{Al}_2\text{O}_3$ . He has found the attenuation to have a  $T^9$ ,  $T^7$ , and  $T^4$  temperature dependence for the longitudinal, fast transverse, and slow transverse waves, respectively, at lowest temperatures. The first two of these dependences are clearly in dis-

agreement with the predictions of the Landau-Rumer theory. We will consider the attenuation of the transverse waves in detail in Secs. III and IV.

The equation for calculating the three-phonon interaction in the presence of finite lifetimes developed by Simons<sup>2</sup> replaces the energy-conserving  $\delta$  function by

$$\langle \sin \Omega t / \Omega \rangle = \int_0^\infty e^{-t/\tau} \sin \Omega t / \Omega \int_0^\infty e^{-t'/\tau} dt' \quad (1)$$

$$= \frac{\tau}{1 + \Omega^2 \tau^2} \quad (2)$$

Here  $\tau$  is the thermal-phonon lifetime and  $\Omega$  is the energy deficit

$$\Omega = \omega_2 - \omega_1 - \omega \quad (3)$$

where  $\omega_2$  is the frequency of the final thermal phonon,  $\omega_1$  the frequency of initial thermal phonon, and  $\omega$  the frequency of the acoustic wave. The integral in the numerator allows for the decay of the coherent state (through other channels) and reduces the interaction considered. The denominator corrects for the fact that the thermal phonons are not depopulated by the thermalizing collisions. It essentially normalizes the population of the thermal phonons to their equilibrium value. The range of validity of Eq. (1) has been investigated by Leggett and ter Haar.<sup>5</sup>

One can consider Eq. (2) to be a weighting func-